

Final Report for NNX12AR02G

SAMPLE RETURN SYSTEMS FOR EXTREME ENVIRONMENTS

R. M. Winglee, C. Truitt

Department of Earth and Space Sciences

University of Washington

Seattle WA 98195-1310

e-mail: winglee@ess.washington.edu

R. Hoyt

Tethers Unlimited Inc.

11711 N. Creek Pkwy S., Suite D113, Bothell WA 98011-8804

e-mail: hoyt@tethers.com

Abstract. Since the Apollo era, sample return missions have been primarily limited to asteroid surface/solar wind sampling. More comprehensive sampling could yield critical information on the formation of the solar system and the potential of life beyond Earth. Hard landings at high velocity (0.1-1.0 km/s) would enable sampling to several meters below the target's surface, while minimizing the ΔV and mass requirements. Combined with tether technology and new energy absorbing material, a host of potential targets and mission scenarios become viable. In the following we detail the design, development, and testing of a hard impact penetrator/sampler that can withstand the hard impact and enable the sample to be returned to orbit. Tether technology - for release of the penetrator and capture of the sample - eliminates many of the restrictions that presently inhibit the development of sample return missions. We show through component testing and simulations, the proposed design can meet the requirements for a hard impact. Initial field testing shows that a full penetrator system can survive a subsonic impact intact, with the potential for supersonic impacts possible though not demonstrated at this time. A full system design is evaluated, and it is shown that multiple return samples of a few kilograms each is possible (either for sampling different small objects, or from different areas on a single large object) with mass requirements only a fraction of what is required for existing soft landing systems that only return a few grams of surface material. Successful development of sample return capabilities will provide a major impetus for solar system exploration.

1. Need for Technology

Samples returned from a solar system object can yield critical information on the formation of the solar system and the potential of life beyond Earth, but collecting and returning the samples is a costly and complex undertaking. Sample return missions are one of the most challenging problems for space exploration due to the energy requirements to get to the surface, extract the sample, and then return to Earth.

There have only been a few sample return missions since the start of the space age. The *Apollo* era saw the return of sizeable samples from the Moon. In the 1970's, the Russian *Luna* program saw the return of much smaller samples of a few hundred grams and were the first to achieve the sample return by robotic means. Since then, there have only been a very limited number of sample return missions: *Genesis* was the first to collect samples beyond the moon, returning dust collected in the solar wind. *Stardust* returned dust samples from the tail of Comet Wild. *Lunar-A* was a Japanese mission with the objective of returning lunar samples, but

PLANETOID	MASS (10^{20} kg)	RADIUS (km)	V_{esc} ($(2GM/R)^{1/2}$)	V_{orb} ($(3GM/4R)^{1/2}$)
208 Lacrimosa	0.00043	20.5	16.7	8.8
Chiron	0.04	90	77.0	45.3
Mimas	0.37	196.5	159.5	95.9
Enceladus	1.10	252	241.3	145.6
Pallas	2	272	321.7	194.3
1994VK8	4	389	370.4	224.6
Vesta	3	263	390.1	235.5
Tethys	6	531	394.7	240.0
Ceres	10	487	523.4	318.1
Dione	11	561	511.4	311.1
Iapetus	18	734	572.0	348.5
Charon	17	586	622.1	378.5
Rhea	23	763	634.1	386.4
Titania	35	789	769.3	468.9
Pluto	125	1137	1211.0	739.2
Triton	215	1353	1456.0	889.1
136199 Eris	167	581.5	1957.3	1191.0
Europa	480	1565	2022.7	1235.7
Luna	735	1738	2375.2	1451.4
Io	893	1821	2557.7	1563.0
Titan	1345	2576	2639.2	1613.8
Ganymede	1482	2634	2739.6	1675.3
Mercury	3330	2439	4267.7	2609.4

Table 1. Escape Velocities and Orbital Velocities of Solar System Planetoids. The proposed system would be applicable where the ΔV into the surface is less than about 1 km/s

problems with the thruster eventually lead to the cancelation of the project in 2007. *Fobos Grunt* had the objective to collect samples from Phobos, but failed to reach escape orbit after its 2012 launch and crashed back to the Earth. The JAXA *Hayabusa* mission has taken samples of asteroid Itokawa, and the *OSIRIS-Rex* to be launched in 2016 is planned to return samples from asteroid 1999 RQ36, using an extender arm to collect the sample.

The objects these missions sampled share something in common: their ΔV for escape velocity is relatively small at less than about 1.5 km/s. An extended list of solar system objects with comparable escape velocities is shown in Table 1. Except for Titan, all these planetoids have at best trace amounts of an atmosphere, so effects from atmospheric drag can be neglected to first order. In addition, this list contains

several planetoids that have major implications for the formation of the solar system, and/or have a potential impact to astrobiology - i.e. life in extreme environments, and its origins in the solar system. These bodies include: Europa, a moon of Jupiter, which is thought to have subsurface oceans; Ganymede, which is also a moon of Jupiter, and is the only moon with a global magnetic field; Titan, a moon of Saturn, which has a thick atmosphere comparable to that of the Earth; and Iapetus, also a moon of Saturn, with distinctive colorations and strong distortions from possible impact events. The asteroid belts also offers important opportunities with potential economic gain in the form of accessible rare metals.

The concept of sample return missions from hostile environments is not restricted to space applications. There are also important applications in the terrestrial environment. Two such examples include the placement of diagnostic probes in or around active volcanic systems, and around failed nuclear power plants such as the 2011 Fukushima Nuclear Accident. In both cases planes cannot access the region due to dust or radiation hazards. New methodologies are required to access such regions to provide key information crucial to understanding and predicting the evolution of such systems.

The developments supported under this grant for Sample Return Systems for Extreme Environments (SRSEE) seeks to fill this gap through the study and development of a hard impact (high speed) impactor or penetrator from which a sample can be retrieved. In Section 2 we described the overall mission concepts for SRSEE. One of the innovations for the SRSEE is the use of tethers to ensure sample return while at the same time reducing overall mission requirements. These features are discussed in Section 3, while the design of the actual penetrator and testing of individual components is described in Section 4 and demonstrate that the overall component requirements can be achieved. Section 5 describes the construction and field testing of the prototype, including oblique penetration and seismic impact signals. With these results a full flight system was developed and is described in Section 6 with the workings of the tether detailed in Section 7. A summary of results is given in Section 8.

2. Basic Return Mission Scenario.

Return mission scenarios fall into two categories: (a) soft landing and (b) hard impact. The soft landing scenario requires ΔV maneuvers to bring the spacecraft to rest alongside the object. The sample is then taken and delivered to the spacecraft, which then undertakes a thrust maneuver so that it eventually reaches escape velocity and the spacecraft returns to Earth. The process for an asteroid rendezvous requires a total ΔV of less than a few km/s, and can be achieved with existing technology with the propellant mass being comparable to the dry mass of the system which can be a few hundred kg. However, only surface sampling has been performed due to the fact that drilling into the surface requires the addition of a substantial amount of mass and complexity.

The energetic requirements for soft landings become much larger when considering return missions to either the inner planets, or to the satellites of the outer planets. To achieve an orbit with these solar system objects, much larger ΔV 's are required for capture around the object in addition to dropping down to the surface. For example, the Cassini spacecraft has undertaken flybys of Saturn's moons, and there is typically a ΔV between the moon and the spacecraft of between 5 and 10 km/s. There are similar issues for the moons of Jupiter. Mercury Messenger has demonstrated that well-designed orbits can enable eventual capture around the planet. However, once in this orbit, a ΔV of about 4 km/s is required to escape Mercury, and

another 17 km/s is required to reach Earth orbit. Substantial savings in ΔV would be achieved if the returning vehicle does not orbit around the object and instead maintains a flyby trajectory.

The same is true for terrestrial analogues.

However, if a flyby trajectory could be utilized then ΔV requirements could be greatly reduced providing substantial mission savings. In this case the sampler/penetrator has to handle a landing with a ΔV of 1-2 km/s. If this impact can be survived it provides a direct means for subsurface sampling which leads to the scenario in Figure 1. In this scenario, the penetrator/sampler separates from the main spacecraft prior to the encounter with the object. It is given a slightly different ΔV so that it will impact on the surface, and the energy of the impact is used to core out a sample that could be potentially several meters in depth. Because only a fraction of the payload goes down to the surface there is already savings in the required ΔV for the total mission. No drilling equipment is required because the kinetic energy involved in the impact is used to core into the surface and break up the material into collectable sizes. The flyby approach offers the opportunity to visit several solar system objects in the one mission. For example the ESA Rosetta Mission to comet 67P/Churyumov–Gerasimenko will have encounters with several solar objects before it reaches its final destination.

In some applications an orbital insertion such as shown in Figure 2 may be more appropriate. For example, if there is a need to provide detailed radar mapping of the surface or to provide detailed information about a particular region then orbital insertion is required. SRSEE can still add capabilities for this type of mission as the system could allow multiple samples to be taken during the orbit. In addition the tether could be used to toss the return sample on an earthward

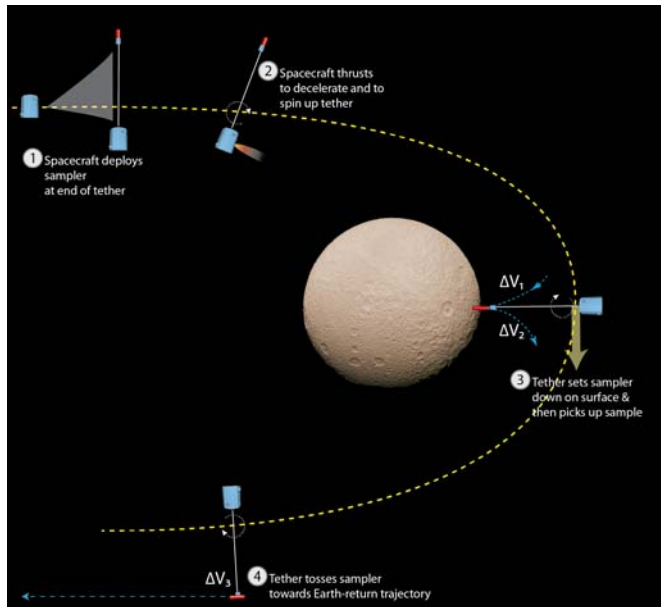


Figure 1. Schematic of the deployment penetrator system for a flyby mission, starting with its (1) deployment of a tether, (2) spin up of the system to minimize the penetrators speed to the surface, (3) hard impact with the surface and recovery of the sample only and (4) recovery of the sample by the main spacecraft.

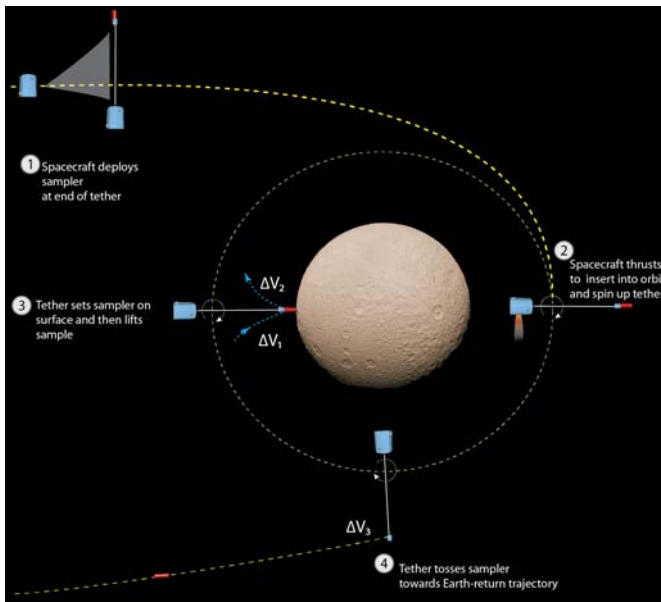


Figure 2. Schematic of the deployment penetrator system for an orbital insertion mission.

back trajectory without the main spacecraft having to leave orbit.

Details of the impact are shown in Figure 3. The kinetic energy of a 10 kg payload moving at a speed of 1 km/s relative to the surface, has nearly 5 MJ of energy or about the energy of 1 kg of TNT. This energy is more than sufficient to produce a hole several feet deep in most of the surface material likely to be encountered in the above planetoids. Feed ports in the nose of the penetrator allow materials to pass into the center of the system where it can be collected by the return sample system.

The return sample sits on energy absorbent material that takes up the bulk of the impact energy, preventing the return sample from being damaged by the impact. Because of the large

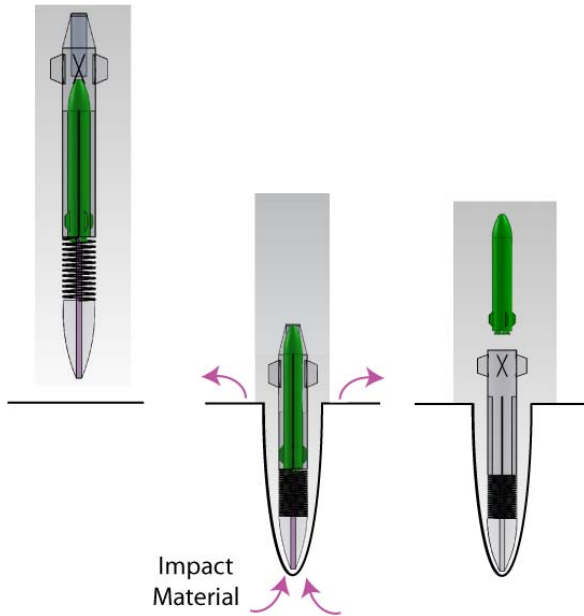


Figure 3. Impact scenario. On impact, the crumple zone is compressed allowing for the safe deceleration of the sample return system. Sample material is forced through a center feed tube that is connected to the return sample system which returns to the main spacecraft.

energies, we wish to minimize the amount of critical electronics onboard that could be potentially damaged by the impact, and hence the use of a tether can not only reduce the ΔV of the impact but provides a simple but robust means fo returning the sample.

In terrestrial applications the return sample system could be replaced by a desired instrumentation package. In this case speeds for the impact are much less at about 100 m/s, as opposed to the 1 km/s for space applications. At these lower speeds, the deceleration would correspond to about 1000 g's and hardened electronics have been known to withstand up to about 10,000 g's.

Our efforts over the period of the grant have focused on demonstrating that (a) survivability of a hard impact is in fact possible particularly with the inclusion of energy absorbing material, and (b) that tether deployment and recovery offer substantial savings over traditional rocket powered landings and launchings. These two innovations together offer potential new capabilities for sample return missions. In the following we discuss the requirements for the penetrator and sample return components and their testing to create a full system that can take multiple deep samples with system masses less than or about that of the present day soft landing systems.

3. Tether Dynamics.

A crucial part of the proposed system is the use of tethers. Utilization of tethers has the important advantages in that they have the potential to:

- provide a propellantless means for slowing the penetrator down to minimize the impact velocity of the penetrator, and thereby minimize total system mass;
- reduce risk of recovery failure since the sample always remains attached to the spacecraft;

- eliminate the need for any electronics and/or fragile flight control system that might be damaged during the impact;
- allow for multi-penetrator systems since the tether can be reused.

In order to quantify the performance of the tether we performed an analysis of the concept of operations (CONOPS) for the configurations shown in Figures 1 and 2. In these rotating tether systems, each segment of the tether must support the centrifugal force due to the mass of the payload, and the tether between that segment and the payload. Consequently, for tethers rotating with large tip velocities, it is necessary to taper the tether along its length in order to minimize its mass. The required mass for a tapered tether depends upon the tip mass and the ratio of the tip velocity to the tether material's critical velocity according to the relation derived by Moravec:¹

$$M_t = 2M_p \sqrt{\pi} \frac{\Delta V}{V_c} e^{\frac{\Delta V^2}{V_c^2}} \operatorname{erf} \left\{ \frac{\Delta V}{V_c} \right\},$$

where erf() is the error function. Note that in Eqn (1), we have multiplied Moravec's equation by a factor of two because his equation calculates the necessary tether mass between the payload and the center of mass of the system, and an equal amount of tether mass is required between the center of mass and the host vehicle end of the system. The critical velocity of a tether material depends upon the tensile strength, the material density, and the design safety factor according to:

$$V_c = \sqrt{\frac{2T}{Fd}}.$$

The exponential dependence of the tether mass on the *square* of the velocity ratio results in a very rapid increase in tether mass once the required ΔV exceeds the critical velocity V_c .

The derived mass fraction, relative to that derived from the rocket equation, is shown in Figure 4 for the cause of the hyperbolic flyby shown in Figure 1. Figure 4a shows the case de-orbit the sampler and then pull the acquired sample up to the spacecraft. For this $2 \times \Delta V$ hyperbolic scenario, the tether approach can reduce the required system mass for bodies with escape velocities less than 770 m/s. Figure 4b shows comparisons for the case where the tether is also used to sling the sample back towards Earth. For this $3 \times \Delta V$ hyperbolic scenario, a tether can provide mass savings for bodies up to about the size of Triton, which has an escape velocity of about 1,500 m/s. For Ceres, which has an escape velocity of 523 m/s, the tether can reduce the mass requirements by 60% relative to a hydrazine thruster system.

Figure 5a shows comparisons for the orbital scenario for the $2 \times \Delta V$ maneuver and Figures 5b shows the results for a $3 \times \Delta V$ maneuver. The threshold for which the tether out performs chemical rockets is the same at about 770 m/s for a $2 \times \Delta V$, and about 1,500 m/s for the $3 \times \Delta V$. However, because the ΔV that is involved for any specific object is reduced as per Table 1 the system yields a competitive edge all the way to objects as large as Pluto for $2 \times \Delta V$ maneuver and as large as Europa for a $3 \times \Delta V$ maneuver.

¹. Moravec, H., "A Non-Synchronous Orbital Skyhook," *Journal of the Astronautical Sciences.*, 25(4), Oct-Dec1977, pp. 307-322.

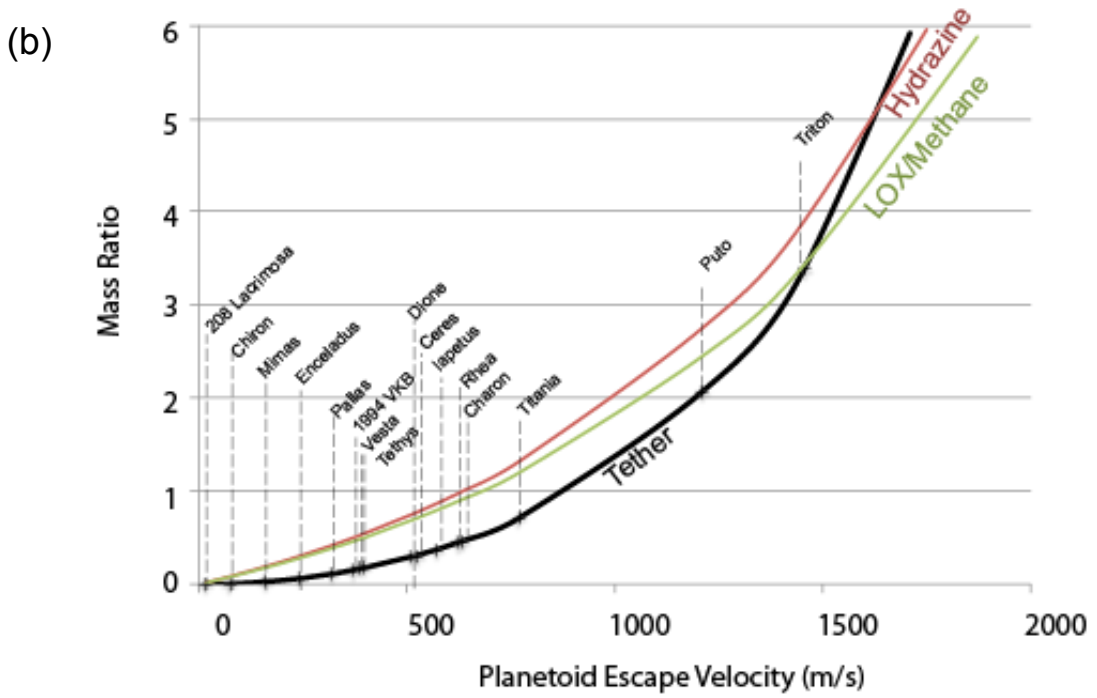
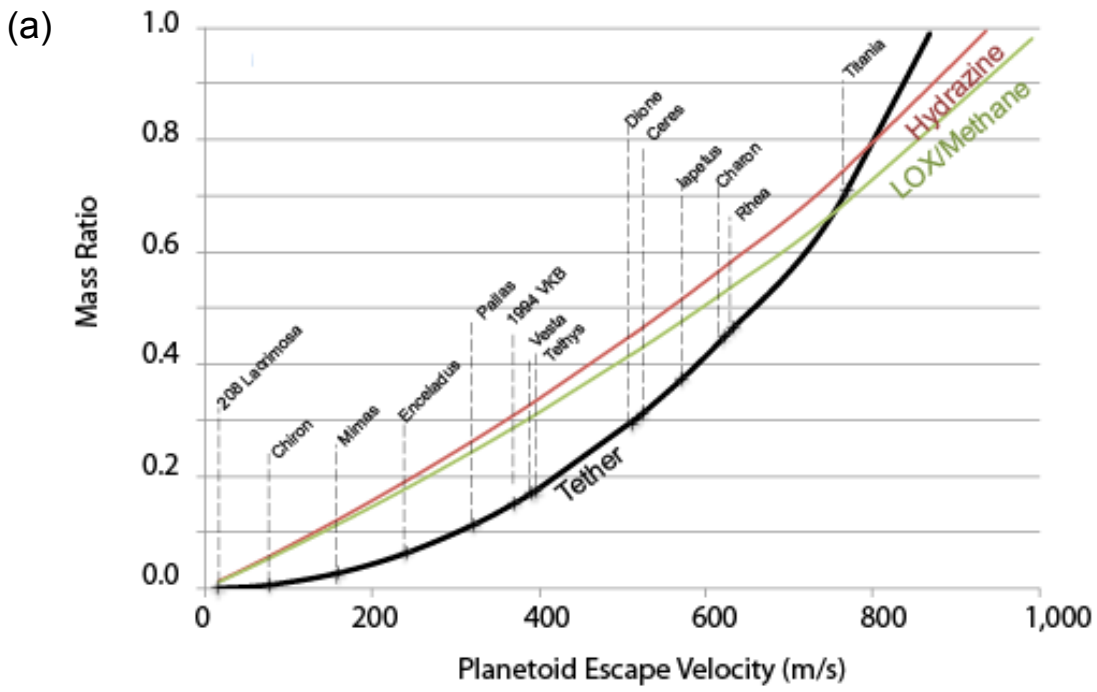


Figure 4. Comparison of the mass ratios for tether and rocket propulsion for (a) $2 \times \Delta V$ and (b) $3 \times \Delta V$ orbital maneuvers for a hyperbolic flyby sampling scenario in Figure 1.

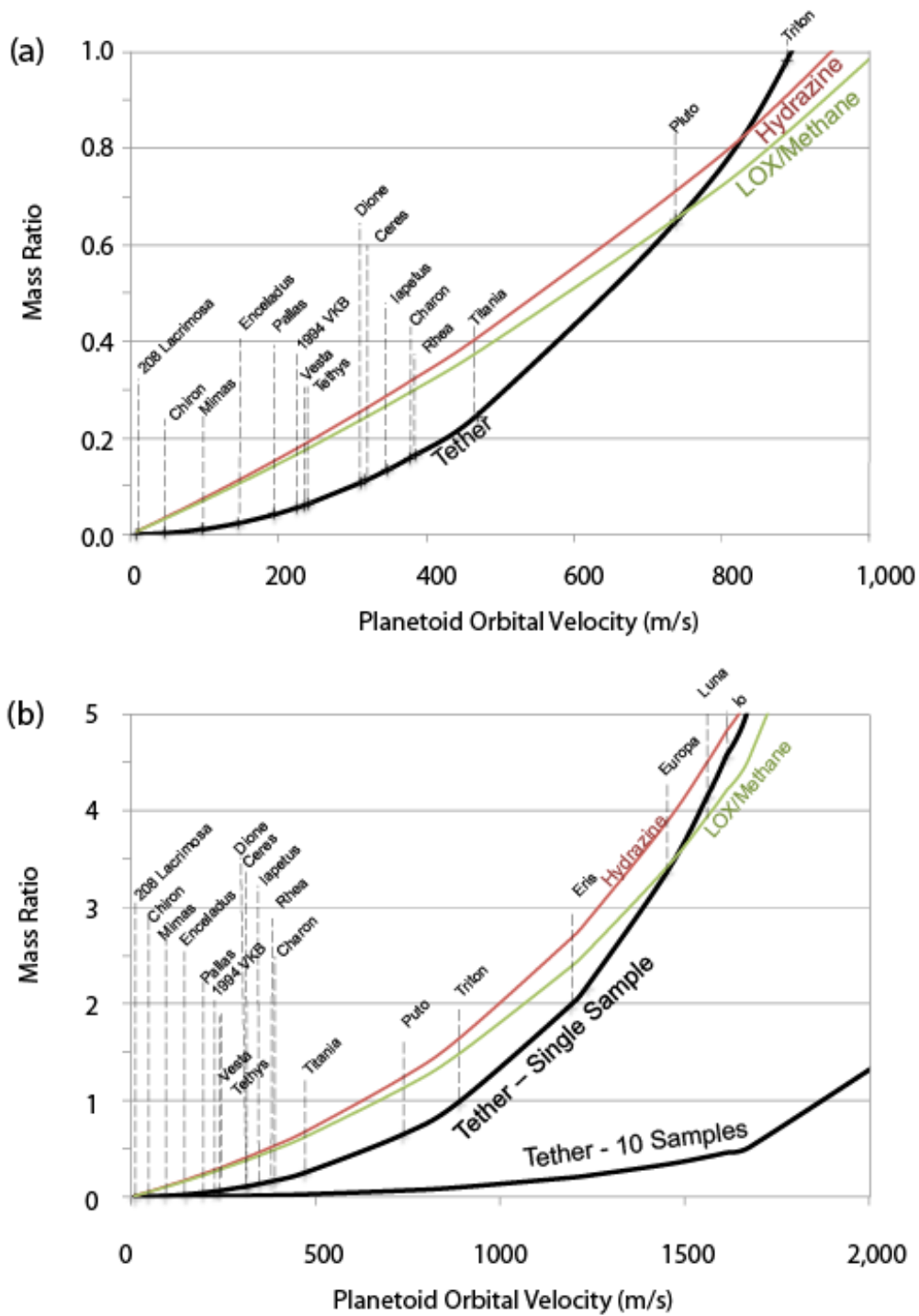


Figure 5. As in Figure 4 except the results for orbital sampling scenario of Figure 2. Also shown in Figure 5b are the results for a mission that involves 10 samples.

The results in Figures 4 and 5 assumed a single sample is taken. However, if multiple samples were to be taken and returned, then the tether option provides huge cost savings over chemical rockets because the tether can be reused. As such, going to multiple objects on a flyby trajectories in a single mission, or taking multiple samples from an orbital mission, becomes possible with little additional cost. This cost savings is demonstrated in Figure 5b where the mass saving for a 10 sample scenario yields a mass ratio of less than 1 for most of the planetoids in Table 1. Thus, the proposed system can provide not only huge cost savings, but it will allow much greater mission flexibility and enable a more cost-effective science return than the typical soft-landing, single site missions presently under consideration.

4. Penetrator Design.

Given the potential costs savings from the tether system, the issue then comes down to whether a penetrator and sample return system can be developed that can take a hard impact up to a 1 km/s. The design that was developed is shown in Figure 6. This system was developed with the specific intention of being able to test it in the terrestrial environment. As such it includes fins for stability of flight in the atmosphere, plus a sustainer rocket system to bring it up to speed. These components would not be needed in space applications.

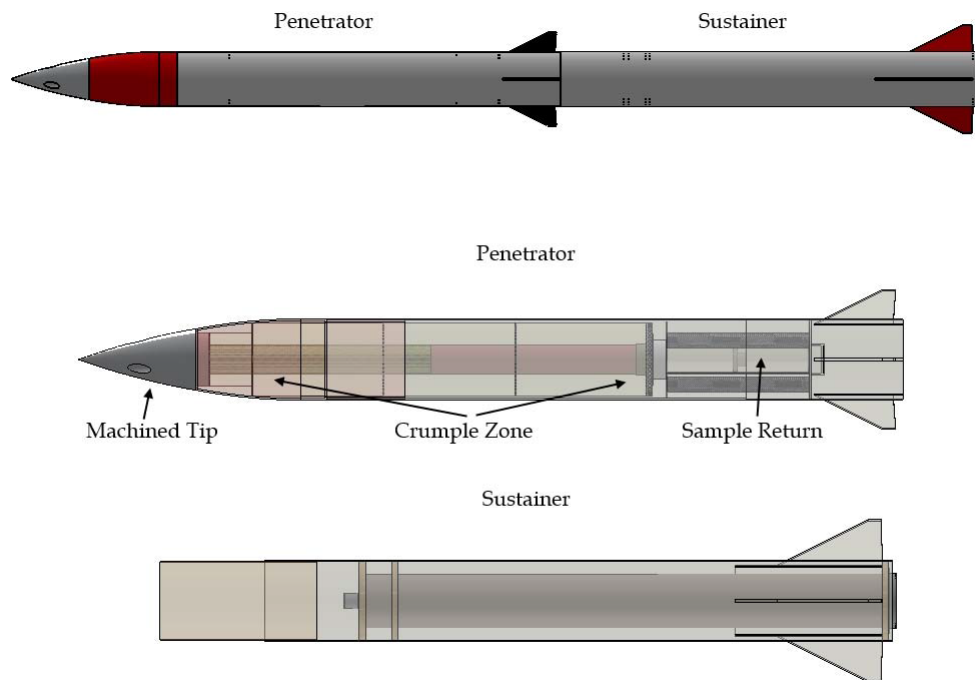


Figure 6. Schematic of the proposed penetrator showing the hardened tip with sample ports that allow material to move up central collecting tube where it is captured with the sample return system which is attached to the tether. The sample return system is supported by energy absorbing material to prevent damage on impact. For terrestrial testing a sustainer with a rocket motor is used to launch the system. Dimension of the penetrator is 6ft long with a 6in diameter.

The penetrator itself consists of a solid nose cone. The hardness of the nose cone has to be higher than the material that it would be flown into. For demonstration purposes we are using an aluminum nose cone which would allow for penetrations into material as hard as calcite (Mohs Hardness Scale of 3). Hardened steel could be used to produce penetration into material as hard as quartz (Mohs Scale of 7). On the flanks of the nose cone, three feed ports were cut to allow for material to flow into a central feed tube. The use of multiple feed ports means that the rocket does not have to go into the ground vertically, but can go in at oblique angles, and at least one of the feed ports will enable material to move up into the center feed tube. This feed tube provides access of the sample material into the sample return system.

The sample return system is seated above a crumple zone. This crumple zone has the requirement of absorbing the energy of the impact of the sample return system so that it sustains minimum damage. To determine the requirements for the crumple zone material, we performed a detailed analysis for the mass budget of the penetrator which is shown in Table 2. The key feature to take away from Table 2 is that the total mass of the penetrator is only about 10 kg, compared with the couple of hundred kg of the satellites involved in soft landings to date, cited in Section 1.

<u>Penetrator</u>	<u>Mass</u>
Low mass Nose Cone Assembly (machined tip & cone)	3.0 kg
Carbon Fiber Airframe (5 ft body tube, coupler, w/ fins)	4.2 kg
Crumple Zone (including divider plates)	1.1 kg
Aft Cradle & Feed Chimney Assembly	0.5 kg
Return Sample System (3 bulkheads, 3 supports, 2in body tube)	1.5 kg
	Penetrator Net Mass: 10.3 kg
Sustainer	
Carbon Fiber Airframe (5 ft body tube, coupler, w/fins)	4.8 kg
Motor Tube, centering rings and retention	0.9 kg
Motor (75mm; Aerotech M1850, 4kg of propellant)	6.2 kg
	Sustainer Net Mass: 11.9 kg
	Total Flight Mass 22.2 kg

Table 2. Mass budget for the penetrator and the sustainer for the system in Figure 6.

Thus, the proposed system not only provides savings and adds to mission flexibility, but it also reduces the mass that needs to go down to the surface, providing additional cost savings. At only 10 kg, the penetrator can in fact be launched at sufficiently high speeds to provide

terrestrial testing with commercially available high power rocket systems. The example in Table 2 uses a sustainer with an M class (7500 Ns impulse) motor, which depending on configuration could be used to produce subsonic to supersonic impacts into the ground. This testing is described in Section 5.

However, before undertaking field testing of the system, two critical components had to have their performance tested against the system requirements. These two components were: (1) the strength of the crumple zone material; (2) the strength of the nose cone to withstand the deformation upon impact with the ground.

4.1. Crumple Zone Testing.

One of the standard materials used in aerospace for crumple zones is Hexcel™, which is



Figure 7. Compressional test stand (left hand side) and control computer (right hand side).

a honeycomb aluminum material that is designed to collapse in an orderly fashion upon impact. As noted above, a 10 kg penetrator going into the ground at 1 km/s has 5 MJ of energy. The return sampler with its lighter mass carries only about 0.75 MJ of energy. Assuming a compression of 1.5 m down the length of the penetrator, the crumple material has to withstand a force of about 500 kN of force before it starts to crumple. The performance of crumple material and other

components of the penetrator were examined through a series of compressional tests using the mechanical press shown in Figure 7.

Figure 8 shows close ups of the Hexcel™ samples in the press, with the initial sample shown in Figure 8a. The condition of the Hexcel™ after compression is shown in Figure 8b. It is seen that the sample retains its overall shape but there is a significant amount of debris that has broken away from the sample and fallen onto the anvil. The compressed sample is also no longer flat, indicating some of loss of structural integrity, and in fact the sample can be easily be broken by hand at this stage. We also considered a sample of Hexcel™ that contained an additive fill material (pattern pending) that was expected to yield greater strength, while still being

compressible and only increasing the total mass by 80%. The image of this sample after

compression is shown in Figure 8c. It is seen that this sample retains its initial shape under compression and it remains flat. In addition the compressed sample still has significant structural integrity and cannot be broken up by hand.



Figure 8. (a) 75×75×16 mm sample prior to compression testing, (b) standard Hexcel™ after compression with debris present around the sample and (c) filled Hexcel™ which shows greater strength and less debris after compression.

The measured compressive load on these samples is shown in Figure 9. The standard Hexcel™ (of original height of 16 mm) is able to hold a maximum load of about 84 kN within the first 0.6 mm. After that the sample continues to weaken, and only holds off 50 kN by the time it has been compressed by about 10 mm. After this point there is an internal failure of the structure which produces a sharp drop in the compressional load. The increase in compressional load after 11 mm of compression is due to the anvil pushing on essentially flattened metal with little structure integrity left.

The results are very different for the filled Hexcel™. Initially there is faster weakening of the sample within the first 0.75 mm of compression, relative to the standard Hexcel sample. This is believed to be due to the fill material stretching the walls of the Hexcel™. However, unlike the standard Hexcel™ the compressional load increases, reaching a local maximum of about 160 kN at 1.6 mm of compression (i.e. about 10% of the initial sample thickness). There is then a short period

of weakening to about 2.25 mm, after which the load continues to increase. The testing was stopped as the load approached 250 kN, the maximum rating of the press.

The maximum of 250 kN is for a 75 × 75 mm cross-section. The expected compressional load for the design (6 in diameter system) is about 780 kN. Thus, the filled Hexcel™ material

exceeds the 500 kN requirement for the desired compressional load on the crumple zone, leading to the absorption of 0.75 MJ of energy by the sample return system.

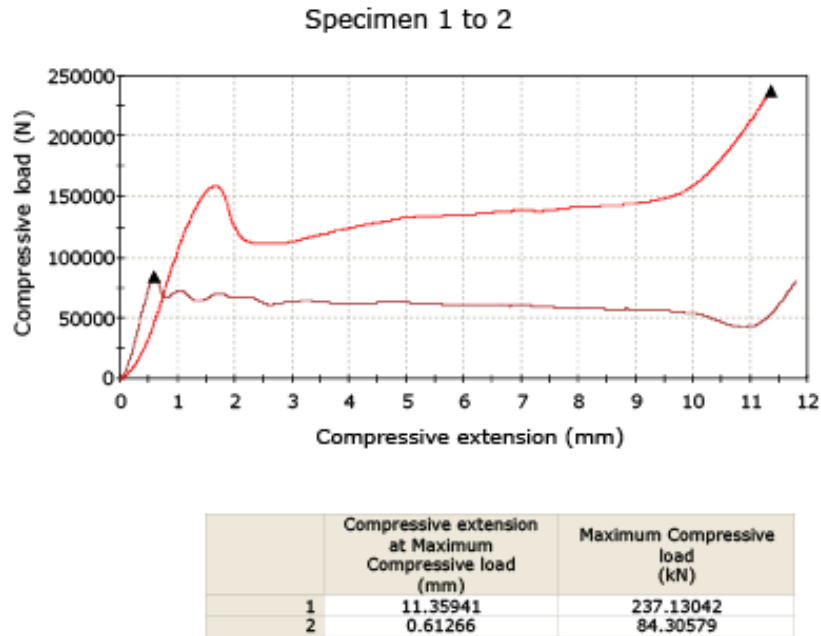


Figure 9. Measured compressional load for the 75×75x16 mm samples in Figure 8. The lower (dark red) curve is for standard Hexcel while the upper (bright red) is for the filled Hexcel™. The latter is able to take more than twice the load of the standard Hexcel™ sample.

4.2. Nose Cone Impact Simulations

The other critical issue that needed investigation was whether the nose cone design could withstand the proposed hard impact. To better address this issue, we created a simulation of the impact of the nose cone with Teflon at an initial speed of 700 m/s using ANSYS software package. On the Rockwell scale, Teflon has a hardness of 50-58, which is comparable to the hardness of aluminum which has a value of 60. This study represents the worst case scenario where the penetrator impacts an object of comparable hardness.

Figure 10 shows the results for the impact of a 30 cm nose cone into a 15 cm block. It is seen that there is some deformation of the point of the nose cone, but this damage does not propagate up the field ports. Moreover, the nose cone is able to penetrate the 15 cm with only the loss of about half its speed. Extrapolating these results we anticipate at least 1 m or more of penetration, assuming that the nose cone material is harder than the impact material.

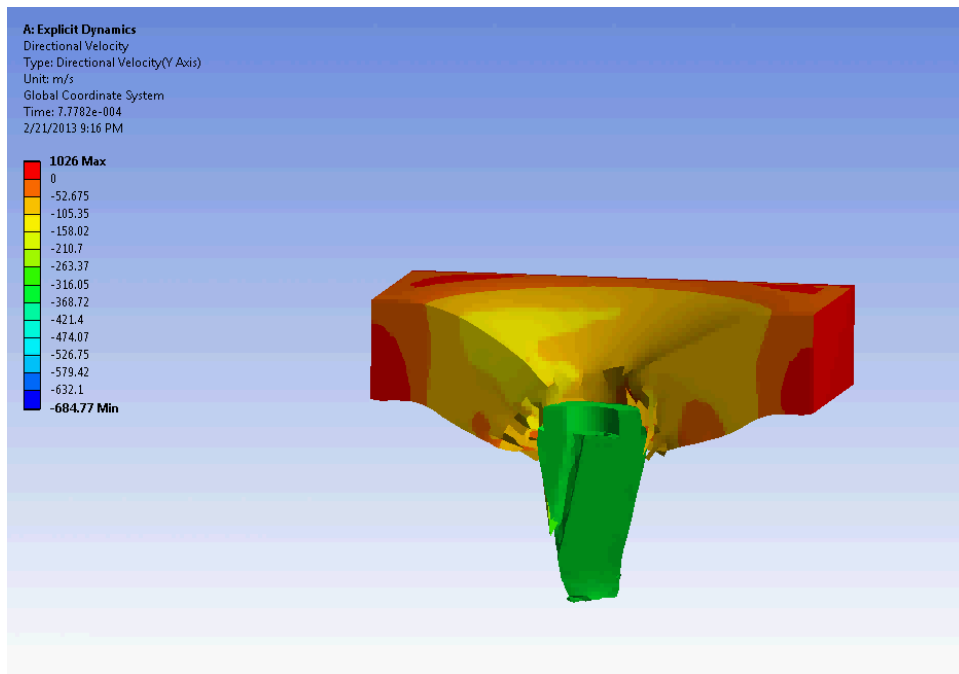
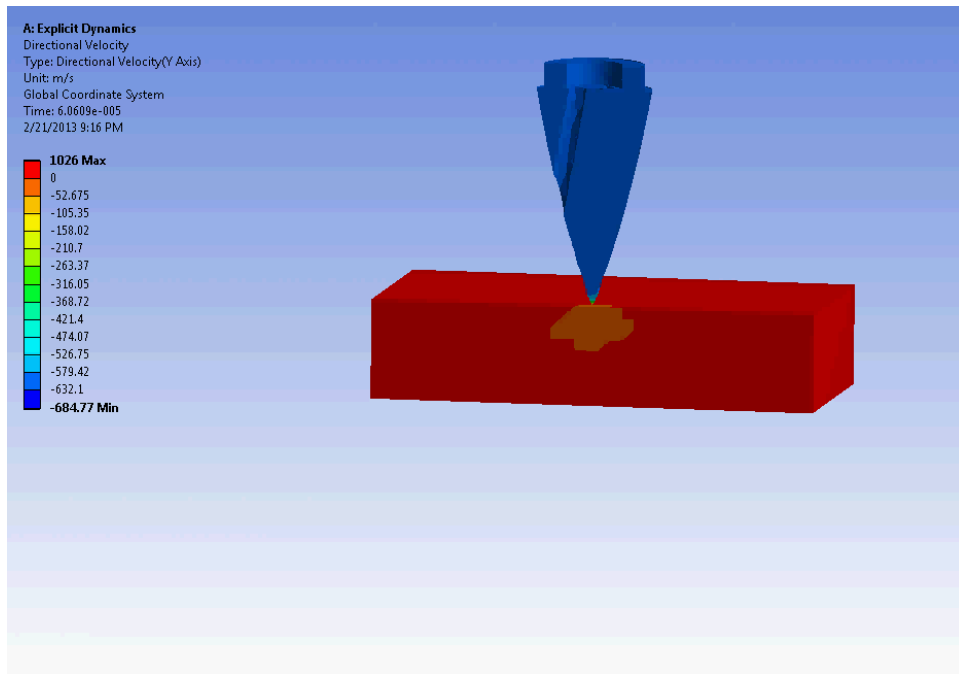


Figure 10. Simulation of the impact of an Al nose cone with sample feed ports impacting a Teflon block. The color contours indicate the speed of the object.

5. Construction and Field Testing of Prototype System.

Given that all modeling and design aspects indicated that the proposed penetrator could achieve the desired goals, we undertook the construction of a prototype system. Figure 11 shows the construction of the nose cone with the sample feed ports that enable sample material to move into the center of the system. The Hexcel™ is then placed around the center collection tube, with body tubing providing an exterior sheath for aerodynamic flight. Two such systems were

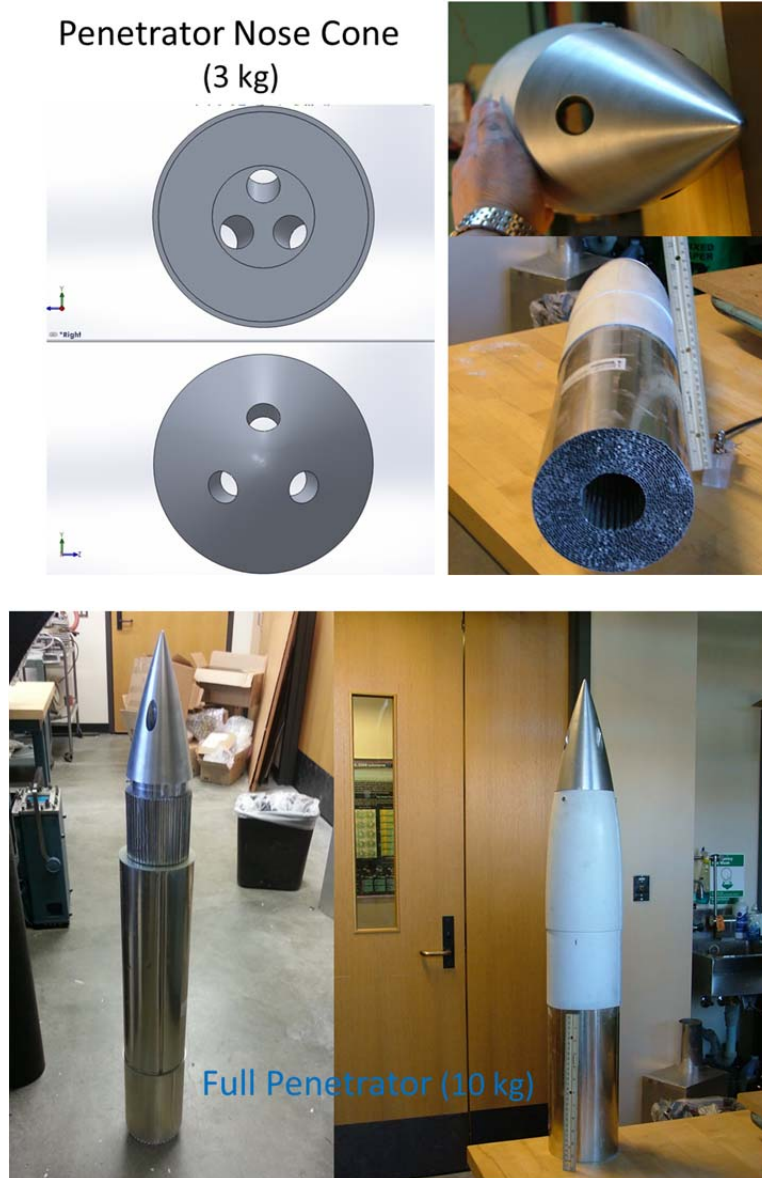


Figure 11. CAD drawings of the nose cone (top left), the actual nose cone (top right) and placement of the Hexcel™ material, and the enclosing of the system with body tubing.

constructed and then taken to Black Rock, Nevada for flight testing in March 2013. The Black Rock area is used for amateur rocketry and has the advantage of including near 100 sq miles of

dry lake bed with no occupants or property, which makes it ideal for the testing. A flight waiver was obtained from the FAA and a land usage permit from the Bureau of Land Management.

As noted in the original proposal, we have been flying rockets at Black Rock for several years and on occasion have had ballistic impacts of rockets due to failed parachute deployment. In such impacts, as shown in the top of Figure 12, there is substantial damage to the rocket system though some components including the tail section can survive. The lower panels of Figure 12 show the results of the impact of the prototype for the case in which the penetrator is lifted up by a sustainer, with separation occurring near apogee of about 5000 ft, and falling ballistically to the ground. Impact speed is about 0.5 Mach, or about 150 m/s.

Inspection of the impact site (bottom left) shows the rear of the prototype intact and projecting out of the playa after the impact. Some of the ejecta materials show stress fractures and some compression. In order to ascertain if the prototype itself was intact we trenched the impact site, as shown in the bottom right of Figure 12. It is seen that the penetrator tip reached a depth of nearly 4 ft, which was more than twice the depth of the crashed rocket system in the top panels. Moreover, the front section of the penetrator is also intact. The only damage on the exterior that was seen was some separation of the body tube from the nose cone.

Another important result from this flight test is the impact angle of the penetrator does not have to occur at near 90 degrees. It has been suggested that non-perpendicular penetration is not possible due to the possibility of snapping the penetrator on impact. As shown in Figure 12, our design has been able to go into the ground at nearly 30° from vertical. This is an important result as it demonstrates that our system is not restricted to perpendicular penetration.

To more fully evaluate the performance of the penetrator, it was taken back into the laboratory and cut open as shown in Figure 13. It is seen that there is very little damage to the interior components. The main damage is some denting of the Hexcel™ material. This lack of damage is consistent with the compressional testing that showed the crumple zone material could withstand forces of 500 kN. At an impact speed of 150 m/s, the force on the material was below threshold, and essentially no collapse of the internal components of the penetrator was expected.

The next step for testing sought to go into the ground at higher speed. This is actually problematic because the energy involved is very much greater, and therefore additional safety protocols are required. One method considered was to use a two stage system where there was an initial boost upwards (similar to the above ballistic test) and then, when the rocket is pointing downwards, ignite a second stage rocket for the higher speed impact. Because we are only using amateur rockets, the downside of this method is that the potential area of impact can be quite large. Given the safety concerns this is not the preferable option.

The other option that we investigated was to fly the rocket using balloons or kites on a tether, so that the exact location of the system at the time of the downward launch could be controlled substantially. Balloon systems offer great stability and less technical challenges, but the payload of 20 kg is fairly heavy for simple weather balloons, and anything larger was too expensive for the Phase I study. High winds that are typical for the Black Rock area also limit the balloon's lift and is only possible at early morning. Therefore, we also investigated the potential for lifting the penetrator by kites, which could then be exactly positioned over the target area. Again, 20 kg is a fairly heavy load for kites, but we found that two power sled kites in tandem could in fact lift the payload. We opted for this procedure for a proof-of-principle flight.



Figure 12. Comparison between impacts from 2012 (top) showing major structural failure with penetration to 22in and the NIAC 2013 test (bottom) where the rocket penetrates to 4ft with a larger impact crater, stress fractures in the playa and minimal damage to the rocket.



Figure 13. View of the internal components of the penetrator after impact. It is seen that beyond some denting of the part of the crumple zone the internal components are essentially intact.

One drawback of the kite system was that the tether that we had was only 5000 ft long. This meant that we could only raise the balloon to 2500 ft in this proof-of-concept flight. It was felt that for the first test of the downward supersonic flight, the lower altitude was preferred so that there was a lower chance that the rocket could go out of range. The drawback of lower altitude was that the penetrator would still be under power from the rocket at impact, so the penetrator would be compressed by both the impact with the ground from below, and from by the powered rocket motor above. At supersonic speeds, the motor could not be ejected while under power. A slight redesign will be considered under Phase II that can overcome this drawback.

Despite the limitation of the experiment, we decided to proceed to at least demonstrate that safe downward flight at supersonic speeds could be achieved, and to attain some initial data on a supersonic impact. Figure 14 shows the lifting of the penetrator up to 2500 ft by the two power sled kites, the ignition of the motor, and the downward launch of the rocket. The air speed of the penetrator at ignition is about 20 mph, and this leads to the peculiar smoke trail. Before the motor comes up to pressure, smoke from the motor is blown horizontally. When the motor is finally up to pressure, the smoke is more energetic and travels more vertically until the point where the penetrator is speeding towards the ground. This combination of effects leads to a question mark pattern.

The flight of the penetrator up to impact is shown in Figure 15. The penetrator is seen to be only 5° from vertical and demonstrates that we can safely position the downward flight into the target area, ensuring the safety of all participants. The estimated speed at impact was about Mach 1.4, or about 420 m/s. This speed is in the middle of the desired operating regime. The ejecta produced by the impact, and the rise of smoke from the impact are seen in Figure 16. The impact ejecta is seen as the dark material that appears around the hole within $1/30$ s after impact (speed of the frames). Smoke is seen to continue out of the hole for a few tenths of a second, followed by a small gap, and then a final burst of smoke (last frame shown). This last burst of smoke probably indicates some obstruction within the hole before it is cleared by the still burning fuel elements of the motor.

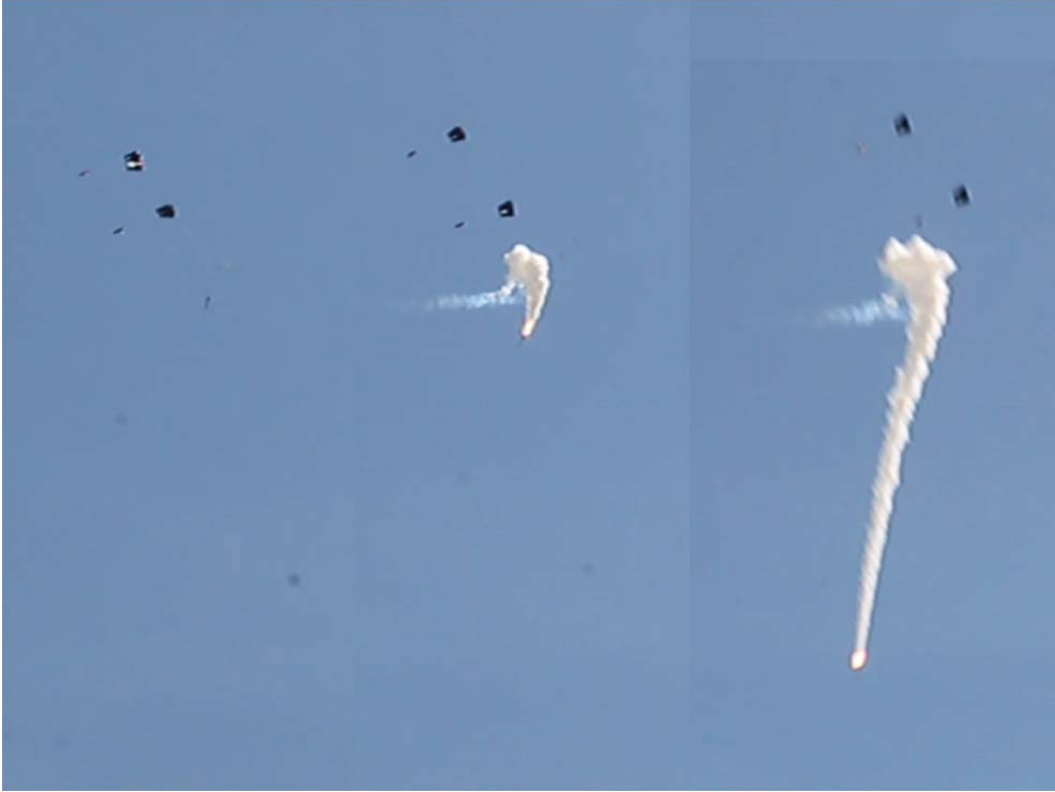


Figure 14. Launch of the penetrator from 2500 ft held up to by two power sled kites.

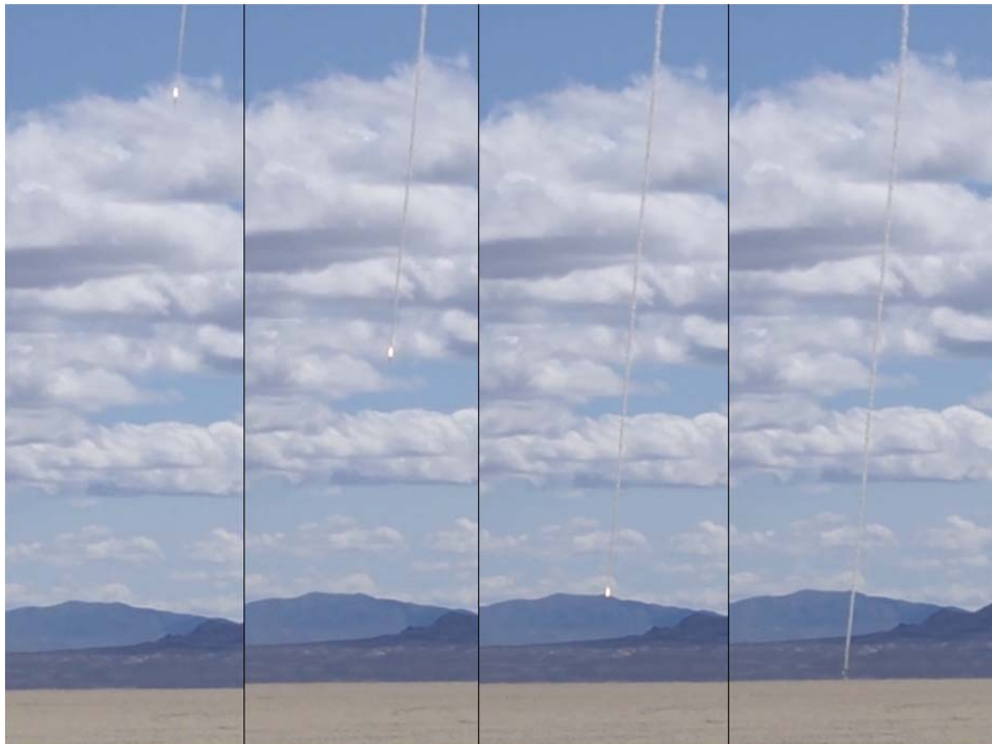


Figure 15. Impact of the penetrator at an estimated speed of Mach 1.4.

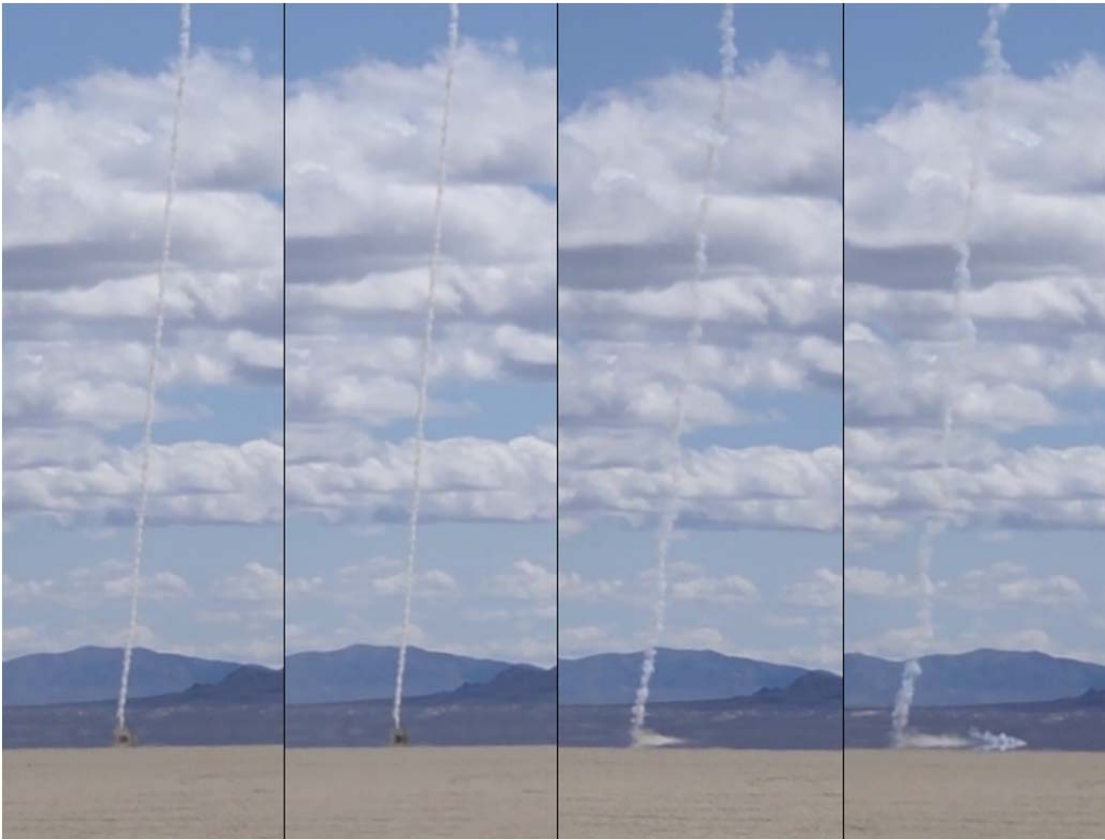


Figure 16. Ejecta and continuing smoke rising from the impact site.

Figure 17 shows close ups of the impact site. There is no evident sign of the penetrator itself, though the site clearly shows the pattern of the fins and rocket body going into the ground. Some of the ejecta shows signs of burning (dark grey) from the rocket motor. The large clump to the left of the hole also showed signs of burning on its underside. The speculation is that this piece was ejected by the burning motor after impact.

Similar to the subsonic case, we trenched the area to ascertain the processes arising from the impact. The nose cone was found intact at 4ft, similar to the subsonic case. However, it was found pushed to the side at a 90° angle from the main entry shaft. This position could only be achieved if the still burning motor overtook the nose cone and pushed it aside. The hole continued to at least 7 ft, but neither the rocket motor nor the rocket body were actually found. There appears to be a cavity the size of the motor going further down but gases from rotting organic material prevented further trenching. A side-by-side comparison of the two entry shafts for the sub and supersonic cases is shown in Figure 18. It is seen that both of the impacts created a well-defined shaft. The supersonic shaft shows strong evidence of modification by the burning motor, as the walls are strongly charred, and there is evidence of some periodic behavior in the hole diameter. The fact the shafts have similar properties suggests that there is potential for survivability of a supersonic impact, but we have to ensure the heavy mass of the motor is ejected clear beyond impact, and this requires a redesign of the test system that could not be achieved within the time and money constraints of the Phase I study.



Figure 17. Impact crater for the powered supersonic flight. The site shows the impact of the fin and body tube though there was no sign of the rocket itself.

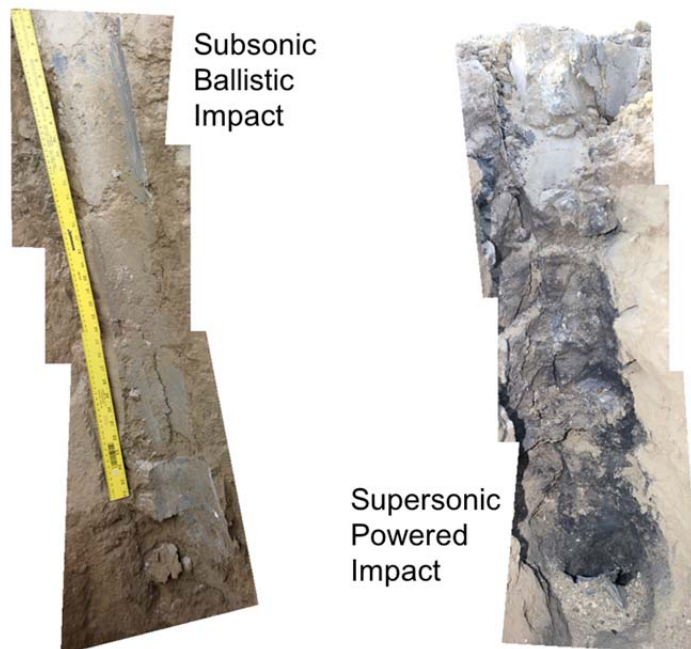


Figure 18. Cross-section of the penetrator holes for the subsonic ballistic and supersonic powered flights. Both show a well-defined hole but the supersonic impact evidence of burning from the rocket motor. The hole for the supersonic case is deeper at about 7 ft.

Despite the damage from the powered motor, this experiment also demonstrated that the sample port system does in fact work as demonstrated in Figure 19. The left hand side shows a top view of the nose cone and the open port of Figure 11 are now seen to be solidly filled with playa material. Some compression of this material was occurred since the density is noted to be about 50% higher than samples taken in the vicinity of the impact site. The right hand side shows a rear view of the same nose cone. Playa material is seen in the central chamber where the sample return material was expected to be collected. There is some asymmetry in the filling which is assumed to be due to the impact being a few degrees off perpendicular. This material was measured to also be compressed though fractionally less than in the nose cone ports. The important point here the field test is able to demonstrate that we are able to get solid material to flow into the middle of the penetrator so that we do have the capability of sample return.



Figure 19. Top and rear views of the nose cone from the supersonic flight. Playa is seen to fill the sample ports and this material is seen in the interior sample collection region.

For the field test, we also deployed a set of 4 seismometers in the area, to test to see if the impact could be measured. While this work was beyond the proposed scope of the project, it provided a chance (at no cost) to obtain critical data for the use of the system in seismic exploration. If successful, not only could we obtain samples from the first several meters of the object, but seismic information obtained by instrumentation in proximity to the impact site could provide a means to sample the deep interior of any object. Unfortunately, due to the setup of the system, two of the seismometers that were run on batteries lost power, leaving only the two stations that were solar powered.

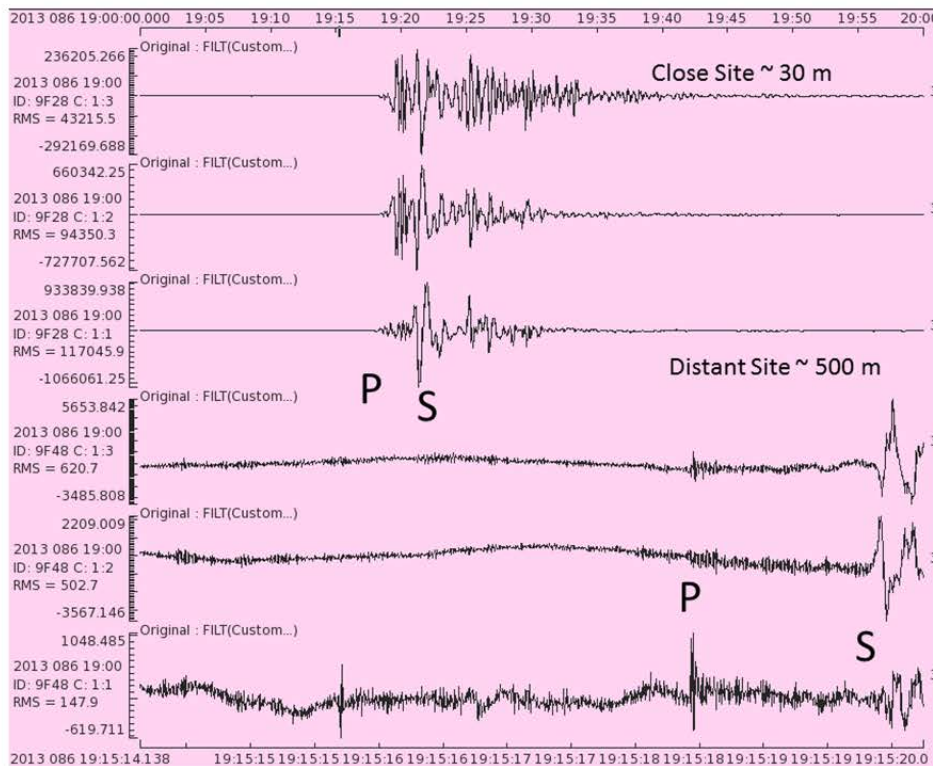
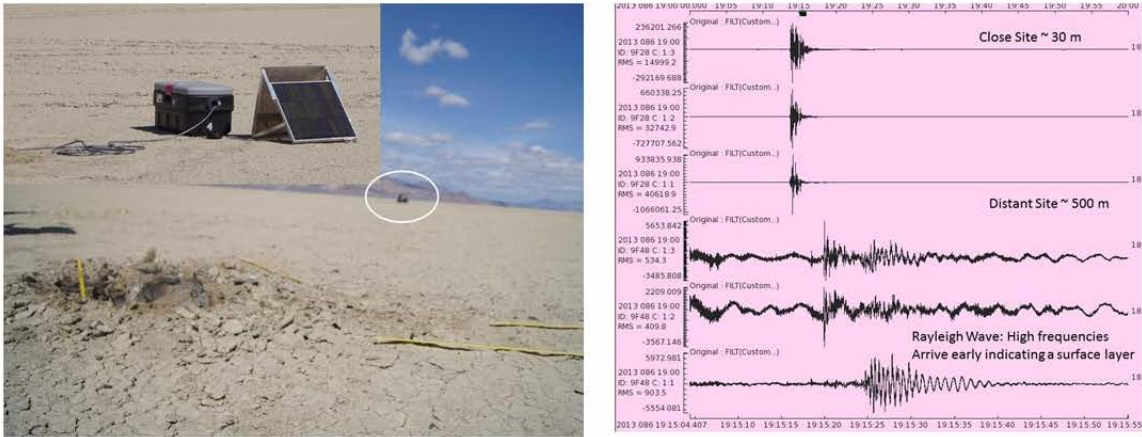


Figure 20. Top left shows the position of one of the seismometers near the impact site, while the top right shows the seismic signal from the 2 working stations at 30 and 500 m from the impact site and bottom panel shows a blown up view of the seismic signals so that the P and S are clearly evident at the two stations.

Figure 20 shows the impact site relative to the nearest seismometer. Due to the aiming allowed by the kite system, the impact occurred within 30 m of one of these seismic stations. The other station was located 500 m away, but both are able to clearly detect the impact. The more distance station is able to detect a clear Rayleigh wave which is indicative of a surface feature in the playa, and is consistent with the trenching that seemed to indicate some type of cavity below 7 ft. The bottom panel of Figure 19 shows a blow up of the P and S waves at both sites. The

derived sound speed is relatively low at about 250 m/s, but this is consistent with the speed of sound for unconsolidated material. More work is still needed to fully analyze the seismic data, but the experiment provides a simple demonstration that the proposed penetrator system - in addition to providing direct sampling - can be used to seismically explore the object's interior as well.

6. A Flight System.

The above results show that a few meters of penetration are possible using penetrators with a total mass of about 10 kg, and that the use of tether technology can provide substantial mass savings for the recovery of the sample if the tether can be used more than once. If one takes note that the mass of the sample return missions to date, those that involved soft landing, are a few hundred kg, then the above results indicate that our proposed system can indeed provide major enhancements for return mission capabilities. To demonstrate this, we undertook a preliminary design for a spacecraft system that could be used to provide multiple sampling of solar system objects. The design is shown in Figure 20.

The system includes several solar panels (blue disks) and assumes that the spacecraft uses electric propulsion. The electric propulsion systems are at the rear, aft of the yellow spheres. The spool containing the tether is forward of the propulsion system, with the tether being black. Six penetrators are racked in a cylindrical configuration. Note that the mass of the penetrators (10 kg each), tether (10 kg), tether spool and motor (10 kg), and support structures (10 kg) comes in at a total of 100 kg. This mass requirement is only a fraction of the mass of the Hayabusa spacecraft, and therefore offers significant new potential without adding significantly to overall mission cost.

The actual system would have the penetrator rotate down from its stacked position and the tether attached to the return sampler inside the penetrator. The penetrator is then released with the tether attached and the system is spun up as per Figure 1 or Figure 2. After the impact, only the sample return system (~ 2-3 kg) is pulled from the surface. At this point the sample could either be tossed by the tether for direct return to the Earth, or it could be pulled onto the spacecraft and stowed in the area where the penetrator was initially stored.

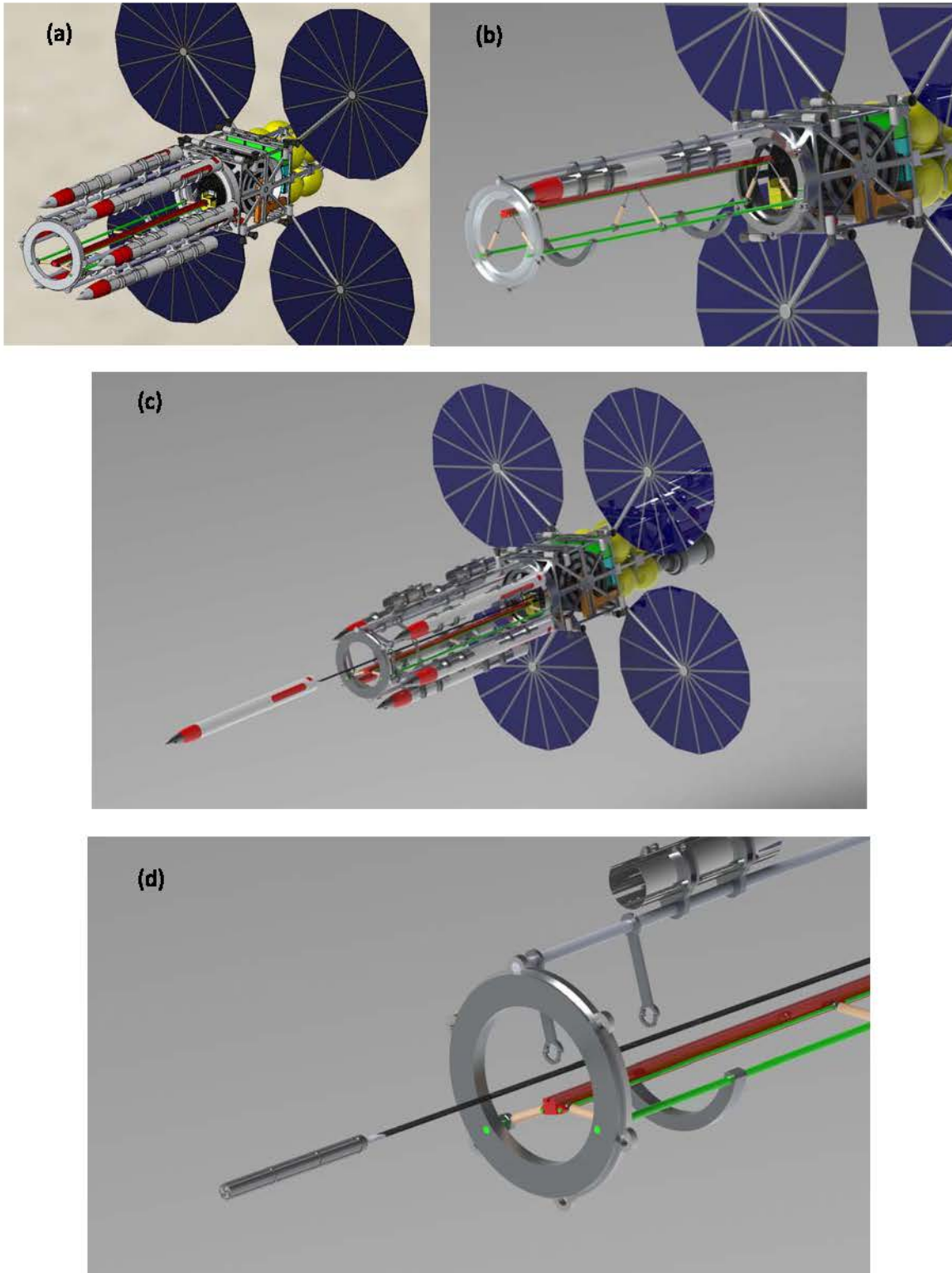


Figure 21. (a) CAD drawing of the proposed spacecraft, (b) movement of one of the penetrator into its lowering position with the attached on the tether, (c) lowering of the penetrator with the tether and (d) return of the sample by the tether to the spacecraft where is can be stored in the initial position of the penetrator.

7. Tether Dynamics.

As the final part of the project we undertook a study of the stresses that would be on the tether during the proposed impacts. Two scenarios were considered: (a) fixed length tether, and (b) a variable length tether. The fixed length tether is the simplest to study but it only has limited applicability. The variable length tether offers significant advantages.

7.1. Fixed Length Tether.

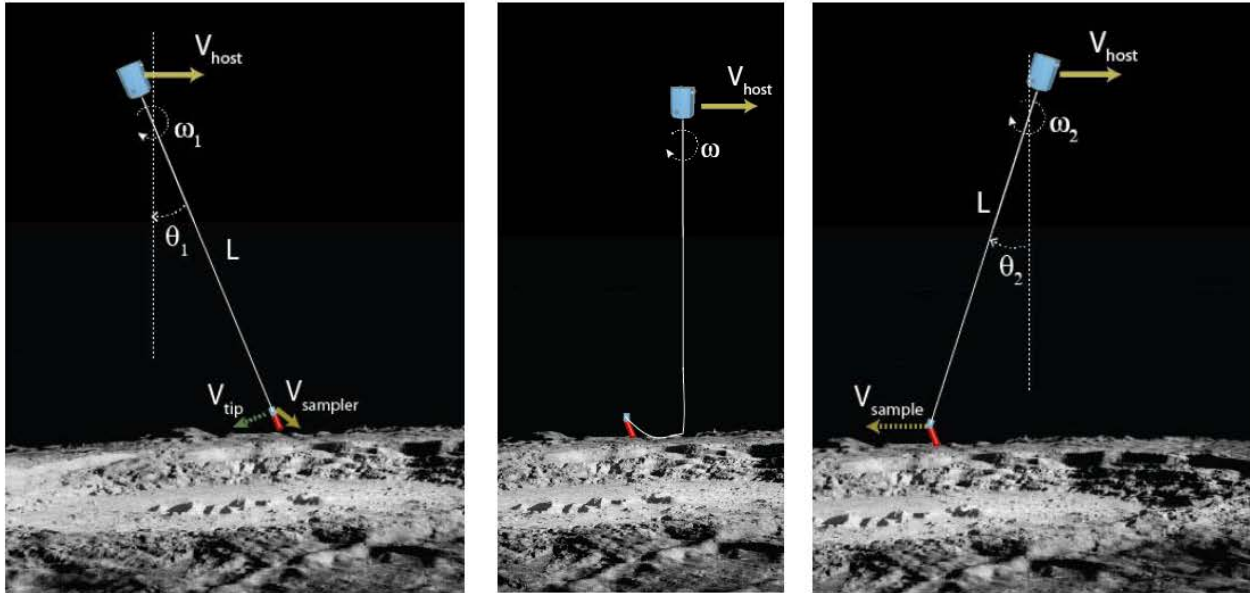


Figure 22. Tethered sample retrieval scenario. LEFT: delivery of sampler; MIDDLE: tether impacts surface ahead of sampler RIGHT: pick-up of sample payload. Solid arrows indicate velocities in planetoid reference frame, and dashed arrows represent velocities in tethered system's reference frame.

Figure 22 illustrates the relevant velocities during a tethered sample retrieval using a fixed-length tether rotating with a tip velocity less than the orbital velocity. The illustration on the left shows the tether system just prior to impact of the sampler. The tethered system is rotating with angular velocity ω_1 about its center of mass, and the sampler at the tip of the tether of length L is moving at velocity

$$V_{tip} = \omega_1 L \quad (1)$$

with respect to the host vehicle. If we assume the mass of the sampler and tether are small, relative to the host spacecraft mass, the velocity of the system's center of mass will be essentially equal to the orbital velocity of the host, V_{host} . The sampler will then impact the surface of the planetoid at a velocity

$$V_{sampler} = V_{host} - V_{tip} \quad (2)$$

If θ_1 is the angle of the tether with respect to vertical when the sampler impacts the surface,

$$\theta_1 = \cos^{-1}(h/L), \quad (3)$$

where h is the host's altitude above the planetoid surface. Then the vertical component of the sampler's impact velocity is

$$V_{sampler, v} = -\sin(\theta_1) V_{tip} \quad (4)$$

and the horizontal component is

$$V_{sampler, h} = V_{host} - \cos(\theta_1) V_{tip} \quad (5)$$

As an example, if the host is at a 30 km altitude orbit around Europa, ($V_{orb} = 1235$ m/s), with a 40 km long tether, with the tether rotating with a tip velocity of 1000 m/s, the sampler will impact when the tether is at an angle of $\theta_1 \sim 41.4^\circ$, with a horizontal velocity of 635 m/s, a vertical velocity of -529 m/s, and a total impact velocity of 827 m/s.

The image on the right of Figure 22 illustrates the subsequent pick-up of the sample payload. This pick-up maneuver will occur when the host has travelled so that the tether angle with respect to vertical is the negative of the impact angle, $\theta_2 = -\theta_1$. At this point in time, the sample payload will be moving at a velocity relative to the host spacecraft of $V_{payload} = -V_{host}$. This payload velocity vector will have components both perpendicular to the tether (assuming for now the tether is straight at this point), and parallel to it.

$$V_{payload, ||} = \sin\theta V_{host}, \quad V_{payload, \perp} = \cos\theta V_{host} \quad (6)$$

For our example of sample retrieval from the surface of Europa, $V_{payload} = 1235$ m/s, $V_{payload, ||} = 817$ m/s, and $V_{payload, \perp} = 926$ m/s. The velocity parallel to the tether will induce a tension spike along the tether, in order to accelerate the sample into rotation around the host vehicle. The magnitude of this tension spike will depend upon the elasticity of the tether, and the damping characteristics of the tether will determine how long the system oscillates due to this tension spike. Controlled deployment and retraction of the tether can be used to more rapidly dampen the resulting oscillations. By conservation of angular momentum, after transient dynamics have dampened out, the final rotation rate of the system will be such that the tip velocity will be equal to $V_{payload, \perp}$. Thus the tether must be sized to support the loads resulting from rotation of the payload mass at this tip velocity, plus the additional transient loads due to the induced tension spike.

In the above maneuver, the tether must support the centripetal force required to accelerate the payload towards the host vehicle by 817 m/s. Because the tether will have a finite elasticity, this acceleration impulse will be spread out over several seconds as the tether stretches to accommodate the load. Typical high-tenacity tether materials such as Spectra and Zylon have an extension at break of only about 2%. However, the process of braiding these materials into a cord typically increases the net elasticity, and can increase the extension at break to approximately 4%. If the tether is designed with a safety factor of 2 for its nominal load under rotation, it will already be stretched by approximately 2% when under rotation. If the system is designed to accelerate a 2 kg sample payload with an additional 1% of tether stretch, or 300 m of

additional stretching, the average centripetal acceleration will be 1112 m/s^2 , resulting in a tension excursion of approximately 2224 N.

An optimally tapered tether constructed of Dyneema fiber, and designed to support a 10 kg sampler at a tip velocity of 1 km/s, would have a mass of approximately 13 kg. The nominal load at the tip, however, is just 334 N. Consequently, the tension excursion due to sample pick-up under this scenario would drive the tether design, increasing the required tether mass to approximately 70 kg.

If the sample capture maneuver is performed with a tether that is longer than the altitude of the host vehicle (so that $\theta > 0$), then after the sampler has impacted the surface, the section of tether near the tip will impact the surface at roughly the same velocity that the impactor did, landing on the surface ahead of the sampler along the host's ground-track, with the impact velocity decreasing as the system rotates towards vertical. This portion of tether therefore will need to be ruggedized to survive this impact, and any subsequent scrubbing and abrasion if it is dragged across the surface. After the host has passed the vertical point above the sampler, the portion of tether above the surface will then begin to pull the tether on the surface back up, accelerating it from rest. The force needed to accelerate the tether up off the ground will help to 'pre-tension' the tether, minimizing transients due to pick-up of the sample payload.

7.2. Variable-Length Tether

In order to mitigate the tension excursion expected with a fixed-length tether system, we developed, analyzed, and simulated an advanced method for tethered sampling that uses deployment of additional tether just prior to impact of the sampler in order to better match the velocity of the sampler to the surface velocity. Figure 23 illustrates a concept of operations where a tether that is initially shorter than the host altitude is set into rotation with a tip velocity greater than the orbital velocity. At the point in the rotation when the backward motion of the tether tip cancels the orbital motion of the system, and the sampler is thus moving only vertically downwards, additional tether would be deployed at high speed from the sampler, allowing the sampler to plunge straight down to the surface. As illustrated in the figure, the tether would continue to rotate past vertical, behind the sampler along the host's ground track. Gradual braking of the deployment of the tether from the sampler would enable the system to lift the sample up off the ground in a smoothly accelerating manner without inducing a large tension shock to the tether.

For example, consider a host vehicle orbiting Triton at an altitude of 30 km at a velocity of 889 m/s, with a 29 km tether rotating with a tip velocity of 1000 m/s. When the tether reaches 27.25 degrees from vertical, the backwards rotation of the tether tip will cancel the horizontal motion of the system, and the sampler will be moving only vertically with respect to the surface. A tether deployer on the sampler then begins paying out tether at high velocity, allowing the sampler to drop down towards the surface. Approximately 5 km of additional tether length would need to be deployed to allow the sampler to impact the surface with a velocity of approximately 475 m/s. The angular momentum of the tether would carry the bottom portion of the tether behind the impact site, and the tether will likely have a significantly bowed shape. Immediately

upon impact, the system would cease deploying tether. It is expected that the bowed shape of the tether at this point will enable the tether to lift the payload up off the surface in a gradual manner, minimizing tension excursions on the tether.

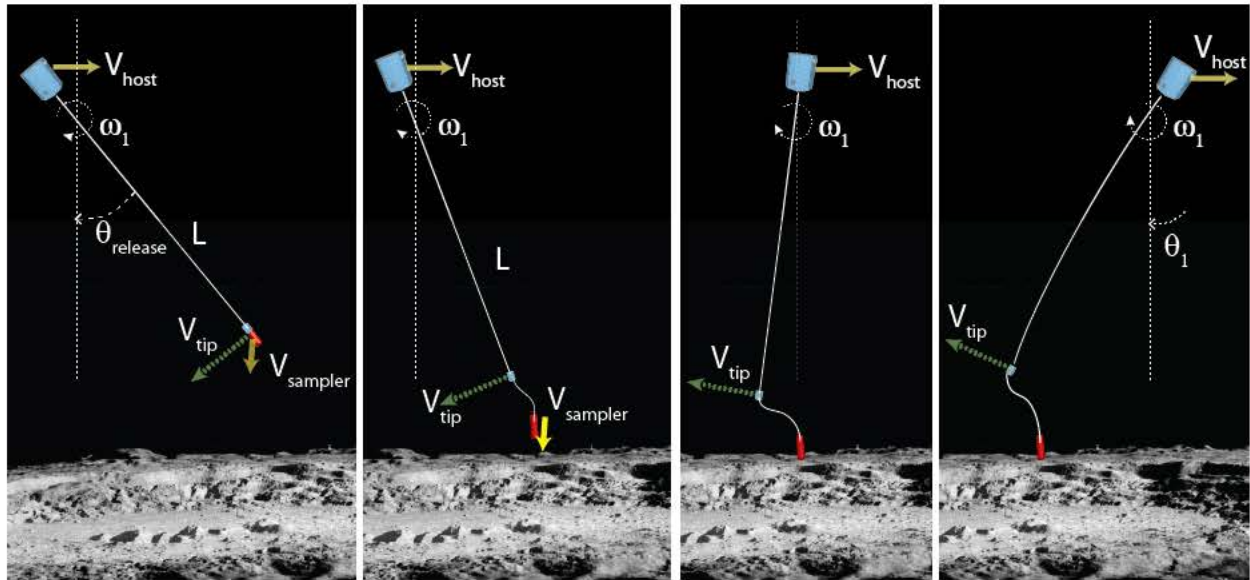


Figure 23. Deployment of additional tether from the tip of a system rotating with tip velocity greater than orbital velocity.

To evaluate the effects of this tether deployment maneuver upon the peak loads experienced by the tether, we simulated the tethered sampling maneuver using TetherSim software code, which integrates orbital dynamics propagators with tether cable dynamics models as well as models for other relevant physics. Figure 24 through Figure 27 show data for tether tip velocity and altitude, deployed tether length, and maximum tether tension during the maneuver. In this simulation, the tether was set into rotation with a tip velocity of 1000 m/s, an initial length of 30.5 km, and at 68 seconds into the simulation, when the tether was aligned approximately 28° from vertical, additional tether was deployed from the sampler at the end of the tether at a rate of 120 m/s, until the sampler impacted the surface of the moon.

This rapid deployment of tether enabled the sampler to impact the surface essentially vertically at a velocity of approximately 450 m/s. Approximately 15 seconds later, the tether picks the sample payload up off of the surface. For simplicity this simulation, assumes that the payload has a constant mass of 10 kg, whereas in reality the intent is to pull only 2 kg off the surface so the actual force on the tether at extraction is significantly overestimated as is the required breaking strength and mass of the tether. In this maneuver, the acceleration of the payload is more gradual than in the fixed-length tether maneuver, and the peak tensions on the tether are significantly reduced, to approximately 1500 N. Note that the tension maximum is reached just prior to sampler impact, not during payload pick-up, so the sampler mass will likely drive the required tether mass. A tether fabricated of Dyneema yarn to support this load with a safety factor of 2 would have a mass of approximately 35 kg. For extraction of a 2 kg sample,

scaling would suggest a mass of 10 kg for the tether would be more than sufficient. Further reductions in the required tether mass may be possible with further optimization of the tether deployment maneuver.

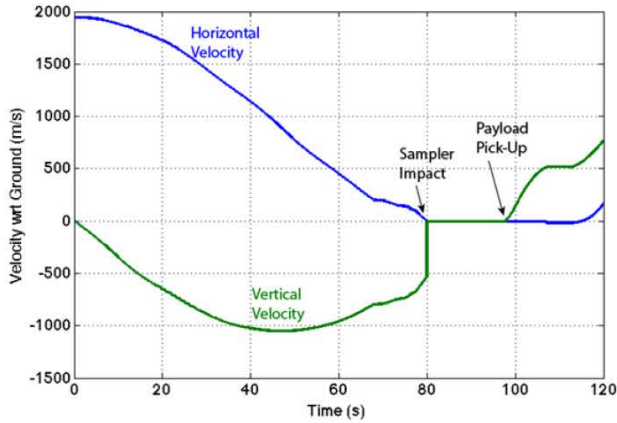


Figure 24. Velocities of the tether tip relative to the surface during sampling maneuver.

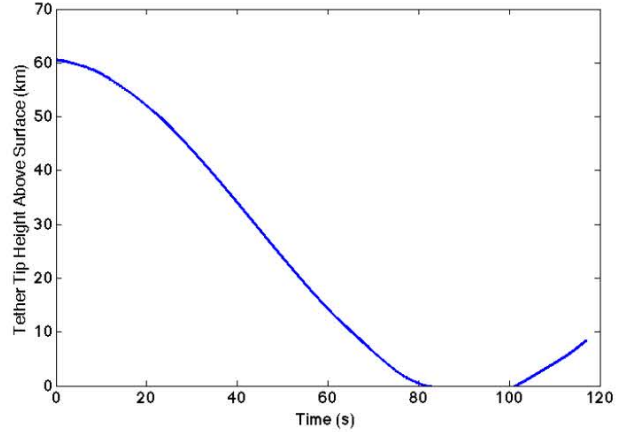


Figure 25. Altitude of the tether tip during sampling maneuver.

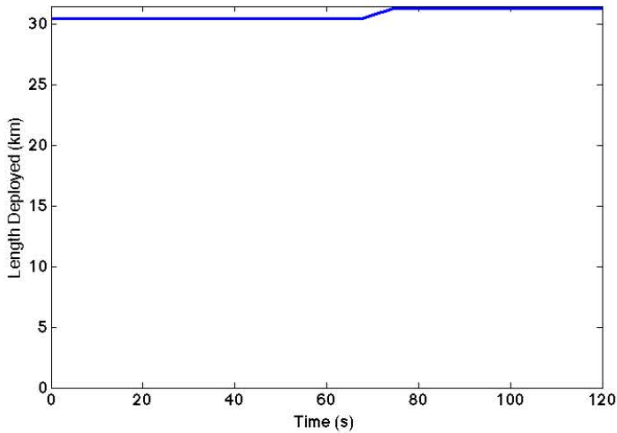


Figure 26. Deployed tether length during sampling maneuver.

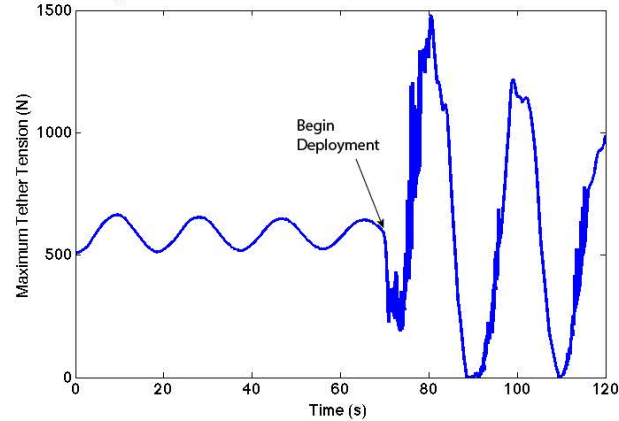


Figure 27. Maximum tether tension during sampling maneuver

8. Summary.

The analysis of the hard impact penetrator systems for sample return indicates that all components involved can meet the necessary requirement to produce substantial new capabilities for sample return missions. The work includes the analysis of the overall mission requirements, the development of new energy absorbing material, tether analysis and penetrator design. This work culminated in the design and building of a prototype and its initial field testing in a dry lake bed in Black Rock, Nevada. The modeling suggests that survivability of sample return system for impacts up to speeds of about 1 km/s is possible and that the sample can be pulled from the surface with existing tether technology. The field tests have demonstrated full survivability at

150 m/s and a means for field test evaluation at higher speeds has been demonstrated, along with the demonstration of sample collection through the feedports and into the main chamber. The full system design indicates that major savings can be accomplished with multiple samples being taken in any single mission, leading to redundancy. This technology will be able for the first time to pull samples of the order of a few kg from depths of a few meters which could greatly enhance our knowledge of solar system objects and the resources therein. Moreover, it offers the opportunity to take multiple samples (from either multiple objects or from multiple areas of a few objects) at little extra cost so that it will provide much greater flexibility and greatly enhance the science return for any given mission.